Cambridge Centre for Computational Chemical Engineering

University of Cambridge

Department of Chemical Engineering

Preprint ISSN 1473 – 4273

Modelling gas-phase synthesis of single-walled carbon nanotubes on iron catalyst particles

Matthew Celnik [1] , Richard West [1] , Neal Morgan [1] ,

Markus Kraft [1] *, Anna Moisala [2] , John Wen [3] ,

William Green [3] , Henning Richter [3] ,

released: 19 February 2007

[1] Dept. of Chemical Engineering /
[2] Dept. of Materials Science
University of Cambridge
Pembroke Street
Cambridge CB2 3RA
UK
*E-mail: mk306@cam.ac.uk

[3] Dept. of Chemical Engineering
MIT
Massachusetts Ave
Cambridge
MA 02139
USA

Preprint No. 44

c4e

Key words and phrases: modelling, population balance, CNT, iron nanoparticles, gas-phase

Edited by
Cambridge Centre for Computational Chemical Engineering
Department of Chemical Engineering
University of Cambridge
Cambridge CB2 3RA
United Kingdom.

Fax: + 44 (0)1223 334796
E-Mail: c4e@cheng.cam.ac.uk
World Wide Web: http://www.cheng.cam.ac.uk/c4e/

Abstract

In this paper we present a simple model for carbon nanotube synthesis in the gas-phase on iron catalyst particles. We include a particle growth model for the catalyst particles and describe nanotube growth processes through carbon monoxide disproportionation and hydrogenation. Models for particle-particle interactions and sintering are also included. Once carbon arrives at a catalyst particle surface it can either dissolve in the particle, until a saturation limit is reached, or form a graphene layer on the particle, or go to form a nanotube. Two models for nanotube inception are considered. The first model allows nanotubes to form once a catalyst particle reaches the saturation condition. The second model only allows nanotubes to form on the collision of two saturated particles. We solve the particle system using a multivariate stochastic solver coupled to the gas-phase iron chemistry using operator splitting. The model is compared to experimental data from a laminar flow reactor and shows promising results under the assumptions made. The model predicts well the nanotube length, and predicts reasonably well the catalyst particle diameter and nanotube diameter of the experimental data. A parameter study is presented in which the carbon monoxide reaction rate constants are varied, as is the fraction of carbon allowed to form nanotubes relative to carbon surface layers. The assumptions of the coagulation and sintering models are also discussed. The model is a first step towards detailed modelling of whole carbon nanotube gas-phase systems, and provides the ground work for future development.

Contents

1 Introduction

Various methods of single-walled carbon nanotube (CNT) production have been reported in the literature, including laser vapourisation [8], arc discharge [7], Chemical Vapour Deposition (CVD) [1] and gas-phase synthesis methods [3, 24]. Within gas-phase synthesis, the High Pressure Carbon Monoxide (HiPco) process is reported [4], but low pressure systems are also used [20].

Moisala et al. [13, 14] and Nasibulin et al. [20, 19, 21, 22] performed gas-phase CNT experiments in a laminar flow reactor. They variously used three feedstocks for iron catalyst particles: iron pentacarbonyl, ferrocene and a hot wire generator (HWG). In their HWG setup they heated resistively an iron filament such that it vapourised and formed iron clusters. Their carbon source was always carbon monoxide (CO). They have presented TEM measured experimental data for primary particle size, CNT diameter and CNT length [20, 22] which is scarce, yet very important for model validation. Carver et al. [4] also present this information and state the difficulties of obtaining such data, as CNTs tend to bundle together on TEM grids.

Several authors [6, 11] have presented molecular dynamics (MD) simulations of CNT formation and early stages of growth which can provide detail of early CNT shape as well as saturation conditions of catalyst particles. However, MD simulations are computationally very intensive and impractical for the calculation of bulk CNT properties such as diameter and length distribution. Scott and Smalley [28] and Scott et al. [29] used a lumped cluster model and a sectional technique to solve a HiPco CNT system. They used a simple kinetic model to simulate CNT formation by counting the number of carbon atoms in a CNT cluster. Their work highlights the difficulty in simulating CNT systems using sectional techniques as they had to alter their model to accommodate the solution method.

Stochastic techniques have been used to study the population balance of soot formation in carbon systems, such as premixed laminar flames [2]. These techniques do not suffer from the numerical diffusion inherent in sectional methods [30], and are able to solve multivariate population balances without additional model constraints. A stochastic solver has been successfully coupled to a deterministic solver for the gas-phase chemistry [5]. This allows stochastic simulations to compete in an area only accessible before by sectional methods. The disadvantage of these techniques is the additional computational time required for solution, though various algorithmic enhancements have been developed [25].

Wen et al. [31] presented a gas-phase mechanism for the growth of iron clusters from iron pentacarbonyl in shock tubes. While the ion pentacarbonyl chemistry was not required for this study, the mechanism describes the growth of iron clusters in the gas-phase including up to seven atoms and the formation of Fe-CO compounds, which are relevant for this study. This mechanism was used throughout this study.

CO disproportionation (Boudouard reaction) and hydrogenation are widely suggested as the mechanisms of CNT growth from a CO source [3, 24, 12, 21]. Nasibulin et al. [22] have presented in several papers a model for formation of CNTs and carbon layers on metal nanoparticles. Carbon is said to deposit on the particle surface via the metal catalysed disproportionation and hydrogenation of CO. This carbon then diffuses into the particle until a saturation point is reached. Carbon then begins to accumulate on the surface

as a graphitic layer from which a CNT can grow. Height [9] suggested a CNT inception model by which a CNT only forms when two saturated particles collide. These models form the basis for the current work. The exact process by which the CNT then forms is still a matter for debate, for example Maiti et al. [10] propose a model based on the formation of heptagons in the graphene layer through which carbon can migrate out of the layer into a CNT.

The purpose of this paper is to demonstrate a working model for CNT growth in gas-phase systems including the solution of particle dynamics and growth processes. We first describe our model for CNT formation and growth including assumptions. We then outline the test case chosen for model validation and compare the simulation predictions with experimental results for primary particle size, CNT diameter and CNT length.

2 Model

A model for the formation of carbon nanotubes on iron catalyst particles was developed based on the current understanding of the underlying processes. The model includes a description of carbon deposition on iron particle surfaces, the growth of nanotubes and monolayers on iron particles and the rules governing particle-particle interactions.

2.1 CNT Growth Model

Two processes have been identified which transfer carbon from gaseous CO to catalyst particles, particularly iron. These are CO disproportionation (Boudouard reaction) and CO hydrogenation [3], given as equations 1 and 2 respectively:

$$2\mathrm{CO} \rightarrow \mathrm{CO_2} + \mathrm{C_s} \quad r = kS_{act}[CO][CO] \tag{1}$$

$$\mathrm{CO} + \mathrm{H_2} \rightarrow \mathrm{H_2O} + \mathrm{C_s} \quad r = kS_{act}[CO][H_2] \tag{2}$$

$$S_{act} = S_0 - S_{ml} \tag{3}$$

S_{act} is the exposed metal surface area of catalyst particles and is defined by equation 3. S_0 is the total particle surface area and S_{ml} is the surface area of the carbon monolayer (defined later). $[\mathrm{CO}]$, $[\mathrm{CO_2}]$, $[\mathrm{H_2}]$ and $[\mathrm{H_2O}]$ are the gas-phase concentrations of CO, $\mathrm{CO_2}$, $\mathrm{H_2}$ and $\mathrm{H_2O}$ respectively. $\mathrm{C_s}$ denotes solid phase carbon whether dissolved in a catalyst particle or in a monolayer or CNT. k is the rate constant. A very simple, temperature-independent rate expression was adopted for both processes whereby the rate was dependent on the available surface area of catalyst particles and the concentration of the reactants. The processes were modelled as irreversible. An initial rate constant of $k = 2 \times 10^{25}\ \mathrm{atoms\,cm\,mol^{-2}\,s^{-1}}$ was estimated from the rate expression for CO disproportionation given by Height [9, page 159]. The same rate constant was used for both

processes, as Nasibulin et al. [22] state that they exhibit similar thermodynamic behaviour, and was varied to test its influence.

Once a carbon atom has arrived at the catalyst surface there are three routes it can take, depending on the conditions: 1 - It can dissolve into the iron particle, 2 - it can add on to a monolayer coating the particle or 3 - it can add onto a CNT growing from the particle. These paths are shown schematically in figure 1. The model assumes each of these paths to be independent and the rates to be sufficiently fast for the processes to be instantaneous. Hence, the dissociation of carbon on the surface is assumed to be the rate limiting step in the model [23]. This assumption should be tested in future work.

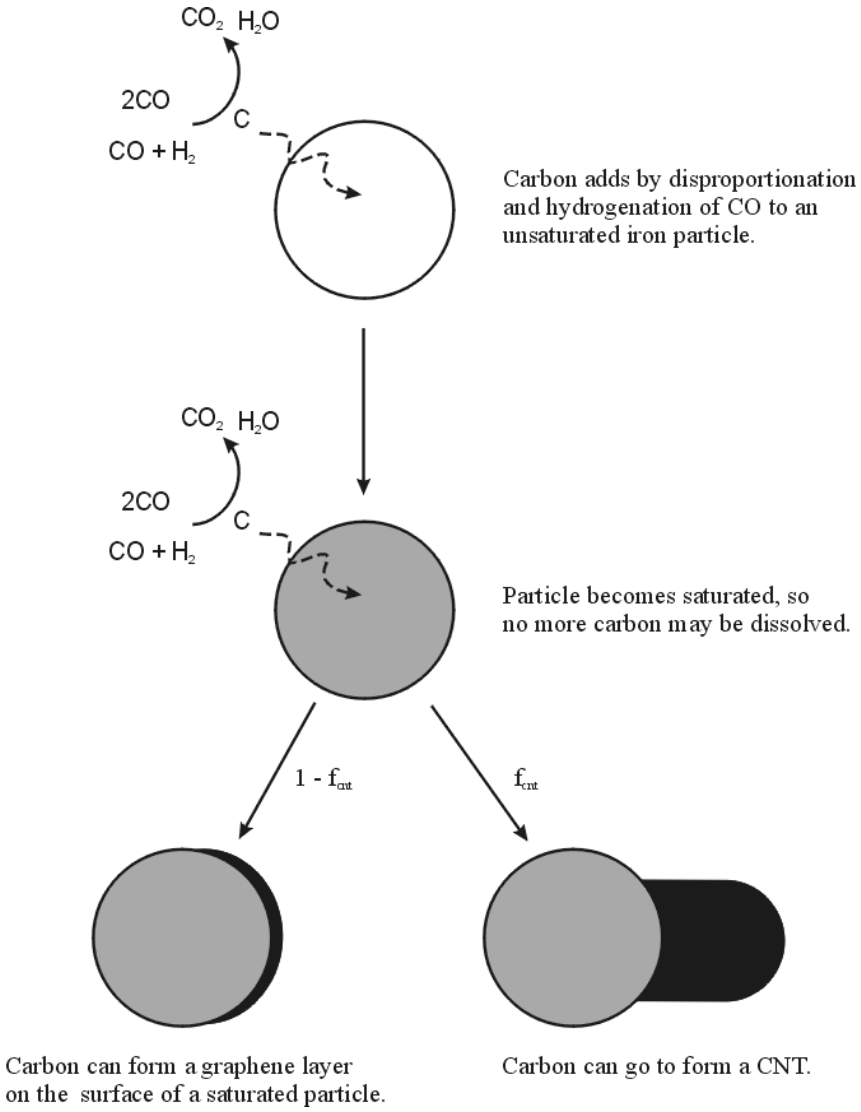

Figure 1: *Schematic of carbon paths on a catalyst particle.*

Carbon was assumed to dissolve completely in an iron particle until the particle reached a saturation condition, beyond which no more carbon can be accommodated. Nasibulin et al. [22] quoted a correlation for carbon solubility in bulk iron as a function of temper-

ature and Moisala et al. [12] quoted a correction factor for small particles. The combined function is given as equation 4 and was used throughout this study. A further study to investigate the effect of saturation and different saturation correlations is noted as future work and was not considered at this time.

$$\frac{[C]_{sat}}{[Fe]} = (0.062305 + 1.176 \times 10^{-4} T) \exp\left(\frac{2\sigma v}{kTr}\right) \tag{4}$$

T is the gas-phase temperature in Kelvin, $\sigma = 0.0172\ \mathrm{N\,cm^{-1}}$ [12] is the surface tension, v is the particle volume, k is the Boltzmann constant and r is the particle radius. Once a particle has reached saturation carbon was assumed to start accumulating on the surface, forming a monolayer or a nanotube. A competition between the rates of monolayer and CNT growth was taken to dictate the point at which a CNT would form. Two models of CNT inception were considered in this work. Model I allows CNTs to grow from a particle as soon as saturation is achieved. Model II requires that two saturated particles collide in order to form a CNT. This is the hypothesis of Height [9]. All collisions in this model result in the formation of a CNT. CNT diameter was kept constant once formed, and was given the value of the primary particle diameter, $6v/s$ [27], at the time the CNT first appeared. v is the particle volume, and s is the particle surface area.

Before a particle reaches saturation the rates of dissolved carbon atom addition (n_{dis}), CNT carbon atom addition (n_{cnt}) and monolayer atom carbon addition (n_{ml}) are given by equations 5 and 6.

$$\frac{dn_{dis}}{dt} = kS_{act}\left([CO]^2 + [CO][H_2]\right) \tag{5}$$

$$\frac{dn_{cnt}}{dt} = 0, \quad \frac{dn_{ml}}{dt} = 0 \tag{6}$$

It is important to note that these and subsequent rate expressions are only valid for a single particle, or in the limit of an infinite ensemble of particles. They are presented here for clarity. After a particle reaches saturation the atomic carbon addition rates are given by equations 7 to 9.

$$\frac{dn_{dis}}{dt} = 0 \tag{7}$$

$$\frac{dn_{cnt}}{dt} = kS_{act} f_{cnt}\left([CO]^2 + [CO][H_2]\right) \tag{8}$$

$$\frac{dn_{ml}}{dt} = kS_{act}(1 - f_{cnt})\left([CO]^2 + [CO][H_2]\right) \tag{9}$$

The CNTs and carbon monolayers were assumed to have a constant graphitic density of $\rho_c = 1.8\ \mathrm{g\,cm^{-3}}$ and a graphene layer thickness of $\delta_{gph} = 0.034\ \mathrm{nm}$ [32]. These values

were used to calculate the dimensions of the CNTs and monolayers. Hence, the rate of length growth of a CNT is described by equation 10.

$$\frac{dL_{cnt}}{dt} = \left(\frac{m_c}{\pi \rho_c \delta_{gph} d_{cnt}}\right) \frac{dn_{cnt}}{dt} \tag{10}$$

Where m_c is the mass of a carbon atom. The rate of carbon monolayer surface growth is given by equation 11.

$$\frac{dS_{ml}}{dt} = \left(\frac{m_c}{\pi \rho_c \delta_{gph}}\right) \frac{dn_{ml}}{dt} \tag{11}$$

Only one CNT was modelled per aggregate particle, which was deemed a reasonable assumption as, for the cases studied, particles were in low enough concentration to have not formed bundles. All particles were allowed to grow a CNT once the saturation condition had been met.

2.2 Particle Coagulation and Sintering

The transition coagulation kernel presented by Patterson et al. [26] was used for this study. The initial coagulation model developed for this study, referred to as model A, is shown as a flowchart in figure 2. On the collision of an unsaturated particle with a saturated particle the carbon is redistributed over the whole particle and the saturation condition must be reasserted, because both the iron and carbon concentration in the new particle have changed. On the collision of a particle with a CNT and a particle without a CNT the CNT is preserved on the resultant particle. However, the particle may still become unsaturated in this case, preventing further CNT growth until saturation is reestablished. If two particles collide which both have a CNT then we assume that if the smaller CNT is shorter than a critical value - $10\ \mathrm{nm}$ was used in this case - it dissolves into the particle and then adds to the other CNT. Otherwise the smaller CNT detaches from the particle and no longer participates in stochastic processes. This model was tested by setting the critical value to a very large number, hence disallowing the detachment of CNTs. This case is referred to as model C in this paper.

A second coagulation model, referred to as model B, was also tested whereby particles with attached CNTs were not allowed to participate in coagulation events. This should approximate the case where nanotube bundles form in which the particles do not actually touch. It is predicted that the true situation will lie somewhere in between models A and B.

Collisions with lone CNTs have been neglected from this study given that this process is not well understood, and it is anyway likely that they would remain on primary particles rather than detaching from the aggregates. For the purposes of calculating particle collision frequencies CNTs were assumed to add mass but not volume to the particles. This is a particularly unfortunate simplification as the coagulation kernel used was formulated for spherical particles, not for long, thin particles. This was noted as an oversimplification, but in the absence of a better model was taken as a first approximation.

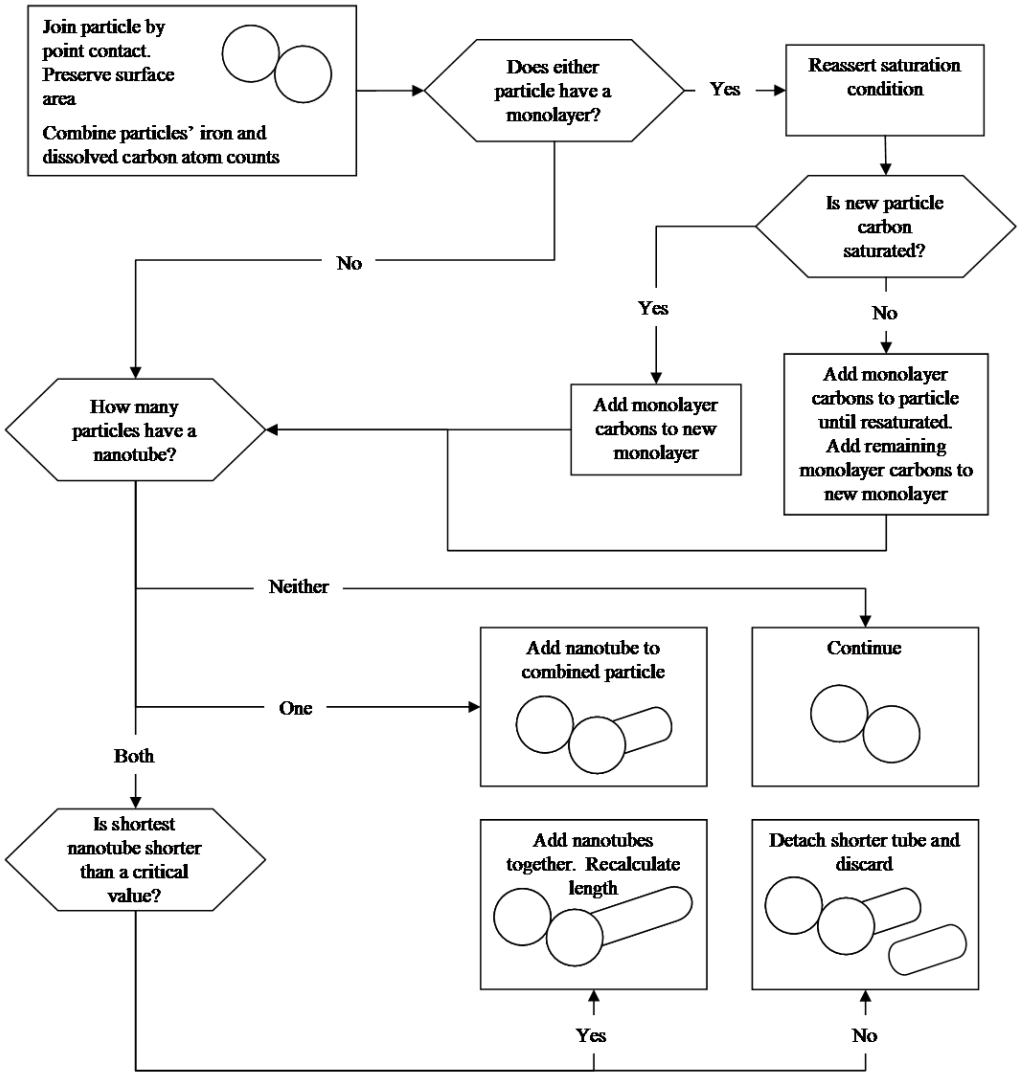

Figure 2: *Flowchart for coagulation process.*

Particle-particle coagulation was modelled as a volume and surface area conserving process (point contact). Surface area was subsequently allowed to change by particle sintering. The particle sintering model is described elsewhere [15] and, due to a lack of knowledge, the sintering parameters for silica [17] were taken as an estimate for iron. It has been observed that metal aggregates in carbon systems have larger diameters than non-carbon systems [18]. In order to test whether the presence of carbon in iron particles stops the sintering process, two sets of numerical simulations were performed: one with the sintering model enabled, and one with the sintering model disabled.

A multivariate population balance solver coupled to the gas-phase chemistry using operator splitting [5] was used. A stochastic particle was defined in the solver as a vector of iron atom count, dissolved carbon atom count, monolayer carbon atom count, CNT carbon atom count, CNT diameter and surface area. All other particle properties were

calculated from these. A surface-volume model [27] was used to provide some shape information about the particles, to allow particle sintering to be modelled and to allow an approximation to the primary particle diameter to be calculated.

2.3 Parameters

Table 1: *Summary of studied parameters.*

Parameter	Description & Range
f_{cnt}	Fraction of carbon which goes to form a CNT in preference to a carbon layer. Studied range: $0.1 - 1.0$.
k	Rate constant for CO disproportionation and hydrogenation. Studied range: $1 \times 10^{24} - 1 \times 10^{27}$.

In order to test the model, two parameters were chosen, which are summarised in table 1. These were CO disproportionation and hydrogenation rate constant, k, and fraction of carbon atoms which go to form CNTs, f_{cnt}; hence fraction of carbon atoms going to form a monolayer is given by $1 - f_{cnt}$. In addition to these parameters the coagulation model was tested with two cases: allowing particles with CNTs to coagulate, and disallowing such particles to coagulate. The sintering model was also tested with two extremes: allow iron particles with a carbon content to sinter, and assuming that the presence of carbon in the particles stops all sintering. A summary of the models used in this study is given in table 2.

Table 2: *Summary of particle models.*

Model		Description
Inception model	I	CNT formation when saturation occurs.
	II	CNT formation on collision of saturated particles only.
Coagulation model	A	All particles stick. Smaller CNTs $> 10\ nm$ in length detach when both particles have a CNT, otherwise carbon added to other CNT.
	B	Particles with CNTs do not stick.
	C	All particles stick. No CNTs detach (all carbon added to other CNT).
Sintering model		Can either be enabled or disabled.

3 Test Case

The experimental work of Nasibulin et al. [22] was chosen because it is a relatively simple system that is easy to model without resorting to CFD. They used a heated, vertical tube as a reactor into which flowed a CO stream and a $\mathrm{N_2/H_2}$ stream in which were entrained the iron catalyst particles. The iron particles were generated by heating an iron filament (hot wire generator, HWG) just inside the reactor. The HWG partially vapourises producing iron particles.

The reactor was simulated using the temperature profile with a maximum wall temperature of $924\,^{o}\mathrm{C}$, as described by Nasibulin et al. [22], for which the coupled solver was modified. Figure 3 reproduces the temperature profile as a function of residence time (Nasibulin et al. gave the profile as a function of reactor position, which required conversion). The residence time was found by linear interpolation of the positional data given by Nasibulin et al. and assuming the flow stream obeyed the ideal gas law. Both the CO and $\mathrm{N_2/H_2}$ stream inflow rates were $400\ \mathrm{cm^3\,min^{-1}}$. The $\mathrm{N_2/H_2}$ ratio was $93/7$. The reactor residence time was calculated to be just under $7\ s$. This is roughly two and a half times as long as the centreline time given by Nasibulin et al., as no velocity profile was modelled.

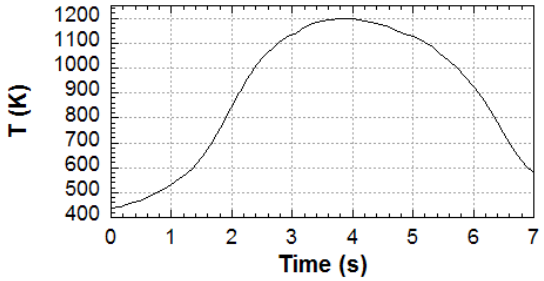

Figure 3: *Reactor temperature profile as a function of residence time.*

Nasibulin et al. reported the output particle size distribution for a similar experiment in which the CO stream was replaced with $\mathrm{N_2}$, such that no CNTs formed. In order to provide the correct initial conditions for the CNT simulations we took a range of initial conditions and modelled this experiment in an attempt to match the resultant particle size distribution. The gas-phase mechanism of Wen et al. [31] includes iron clusters of one to eight atoms. Beyond eight atoms iron clusters are modelled as particles. Simulations were run with initial iron clusters of one to seven atoms monodispersed in the gas-phase with concentrations of $0.05\ \mathrm{ppm}$, $0.5\ \mathrm{ppm}$, $1\ \mathrm{ppm}$ and $2\ \mathrm{ppm}$, from which the HWG initial conditions were estimated.

Figure 4(a) shows that the best fit to the experimental data from our simulations occurs with an initial cluster size of two iron atoms at $0.05\ \mathrm{ppm}$. However, it was found that replacing the second $\mathrm{N_2}$ stream with CO resulted in no particle formation for cluster sizes one to three. It was surmised that this was due to a change in equilibrium of pure iron and Fe-CO compounds in the gas-phase, which were not present without a CO source. Therefore clusters of four iron atoms were chosen to represent the initial conditions of the HWG generated nanoparticle ensemble. Figure 4(b) demonstrates the predicted iron

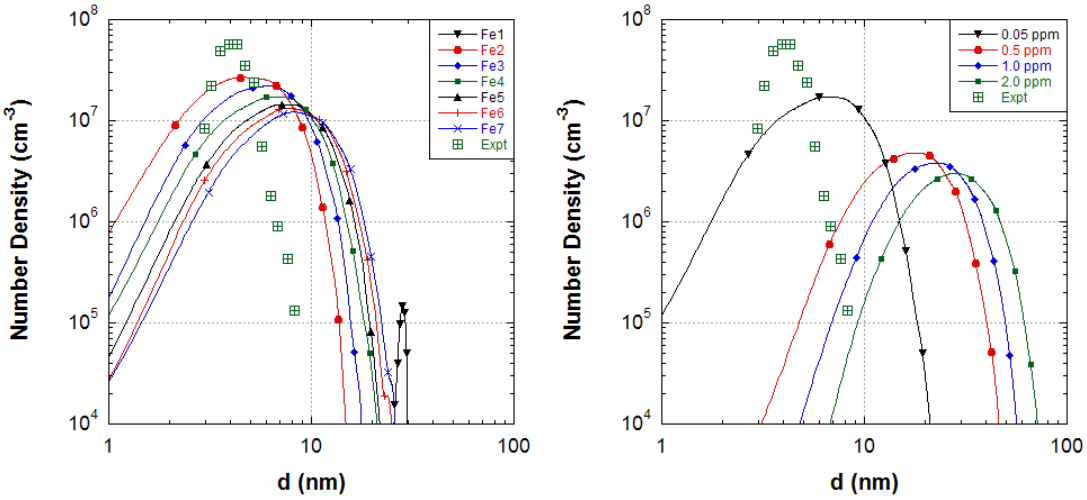

(a) 0.05 ppm

(b) Fe4 clusters

Figure 4: *Particle diameter distribution with a N_2 co-stream for different initial iron cluster sizes. Left figure shows different cluster sizes at 0.05 ppm, and right figure shows different concentrations for a four-atom initial cluster.*

particle distributions as the initial concentration is changed. There is a clear upward trend in mean particle diameter as the concentration increases. It is noted that 0.05 ppm slightly overpredicts the mean diameter, but the difference is not great.

4 Parameter Study: CNT Carbon Fraction

Simulations were performed where the fraction of carbon forming CNTs, f_{cnt}, was varied. As carbon atoms were allowed to form either CNTs or a monolayer, the fraction of carbon going to monolayer is given by $1 - f_{cnt}$. For all these simulations, the rate constants of CO disproportionation and hydrogenation were kept constant at $k = 2 \times 10^{25}$ atoms cm mol^{-2} s^{-1}.

Figure 5 shows the average particle diameter as a function of f_{cnt} for different coagulation and sintering models. There is little difference between the two CNT inception models. When particles with CNTs are allowed to coagulate the particle diameter is overpredicted by an order of magnitude. When such particles are not allowed to coagulate the prediction is much closer to the experimentally observed results, however they exhibit a narrower distribution than the experimental results. Particle diameter is slightly underpredicted in this case, but lies within the standard deviation limits as shown by the dotted lines. This result suggests that it is incorrect to coagulate catalyst particles without considering the CNTs. It is more likely that CNTs would stick together (such bundles are frequently observed experimentally) without the attached catalyst particles joining. A more complex particle description is required to test this. When coagulation was not allowed to occur, sintering had no affect on the results, because aggregates had not formed. When coagulation was

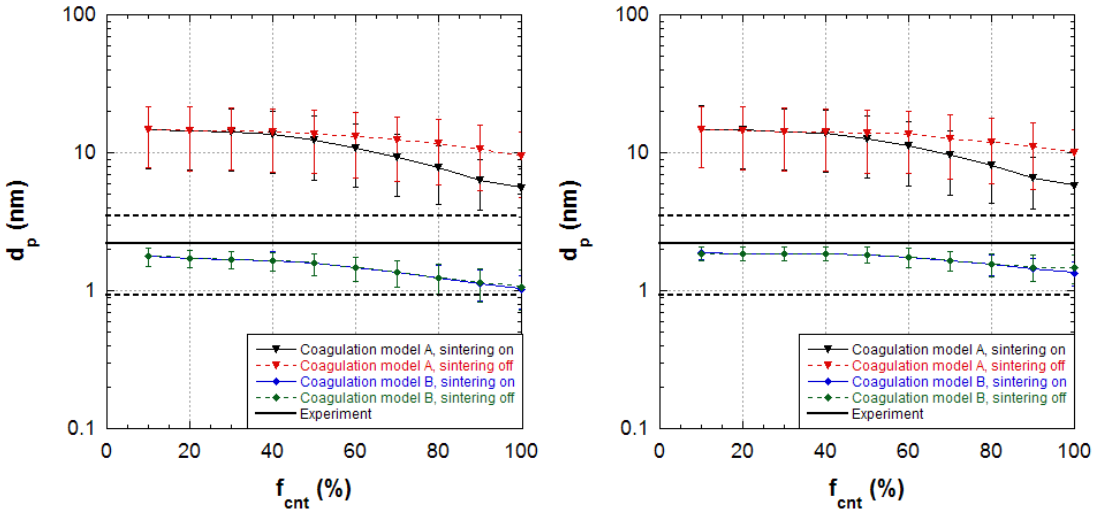

(a) Inception model I

(b) Inception model II

Figure 5: *Average particle diameter after 7 s flow time for different fractions of carbon forming CNTs. Horizontal lines show experimental average (solid) and standard deviation (dotted). Bars show standard deviations.*

allowed to occur, sintering acted to decrease the size of the particles at higher values of f_{cnt}; this suggests that at lower f_{cnt} values more particles are deactivated by complete carbon covering, and hence no longer sinter.

Figure 6 shows the average CNT diameter as a function of f_{cnt} for different coagulation and sintering models. For inception model I, at all values of f_{cnt}, and all coagulation and sintering combinations, the average CNT diameter is underpredicted. The diameter range, indicated by the standard deviations, is also too narrow. As the model gives CNTs the primary particle diameter of the host particle at formation, this result suggests the the model predicts CNTs to form rapidly, before the catalyst particles have grown through surface processes and coagulation. Sintering appears to have no effect on CNT diameter. Changing f_{cnt} has only has an effect for the lower values, which tend to demonstrate slightly larger diameter CNTs, but the effect is not pronounced. For inception model II there is very good agreement between the simulations and the experiments when using coagulation model B. When using coagulation model A the diameters are higher then for inception model I, and lie within the standard deviation bounds of the experimental data. This size increase may be explained by the extra growth time given to the particles before collision of two saturated particles: Bigger particles at CNT inception give larger diameter CNTs.

Figure 7 shows the average CNT length as a function of f_{cnt} for different coagulation and sintering models. For values of f_{cnt} below about 0.3 there is a reasonable agreement between the experimental data and the simulation with coagulation model A. This extends to $f_{cnt} = 0.4$ for inception model II. When coagulation is not allowed the CNT length is underpredicted for all values of f_{cnt}, and grossly underpredicted for low values. Sintering

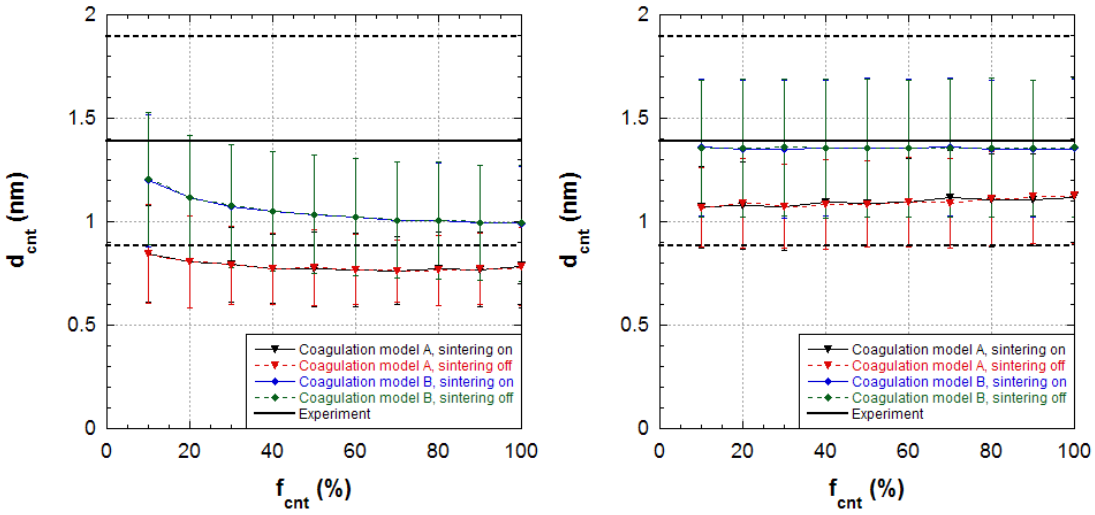

(a) Inception model I

(b) Inception model II

Figure 6: *Average CNT diameter after 7 s flow time for different fractions of carbon forming CNTs. Horizontal lines show experimental average (solid) and standard deviation (dotted). Bars show standard deviations.*

has the effect of reducing CNT length, at larger values of f_{cnt}, which is due to the reduced surface area of a sintered particle compared to an aggregate structure. Inception model II produces slightly shorter CNTs than model I, thereby giving a better fit to the experimental data. Both inception models exhibit the same behaviour otherwise.

5 Parameter Study: CO Rate Constant

Simulations were performed where the rate constant of CO disproportionation and hydrogenation was varied over several orders of magnitude. For all these simulations, the fraction of carbon forming CNTs, f_{cnt} was kept constant at $f_{cnt} = 0.5$.

Figure 8 shows the average particle diameter as a function of CO rate constant for different coagulation and sintering combinations. Again it is observed that with coagulation model A the simulations overpredict the particle diameter by an order of magnitude. The effect of sintering to reduce particle size is observed at lower rate constants, as more time is allowed for sintering before particles are deactivated by carbon coating. When coagulation model B is used the particle size begins to increase as k is decreased. This suggests that CNTs are forming later, hence given the particles more time to coagulate before CNT formation. Coagulation model B also shows a very narrow distribution which does not match the experimental data, even though the average values are close. Otherwise there appears to be no effect on particle size by changing the rate constant, though this is not surprising as the growth of the catalyst particles is independent of the CO processes in the model. Again little difference is observed between the two inception models.

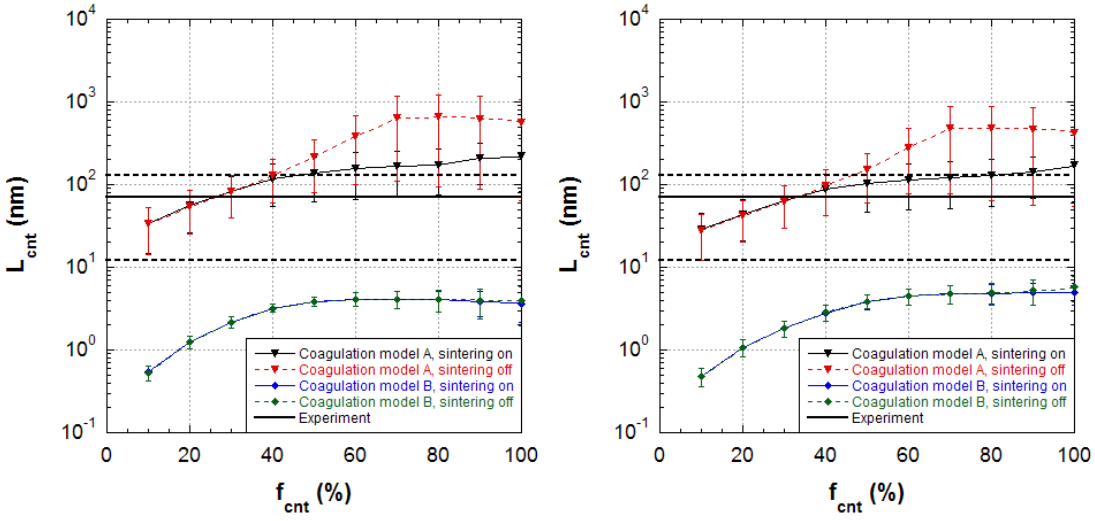

(a) Inception model I

(b) Inception model II

Figure 7: *Average CNT length after 7 s flow time for different fractions of carbon forming CNTs. Horizontal lines show experimental average (solid) and standard deviation (dotted). Bars show standard deviations.*

Figure 9 shows the average CNT diameter as a function of CO rate constant for different coagulation and sintering combinations. There is a clear decrease in CNT diameter as the rate constant is increased for both inception models. At the lowest rate constants all models overpredict CNT diameter. For inception model I the CNT diameter is underpredicted for higher rate constants, given an effective rate of 2×10^{24} to 2×10^{25}, which just reaches our initial estimate. For inception model II there is generally good agreement with the experimental data in the range $6 \times 10^{24} - 1 \times 10^{27}$. Curiously the CNT diameter appears to increase again for coagulation model B at higher rate constants.

Figure 10 shows the average CNT length as a function of CO rate constant for different coagulation and sintering combinations. Again the cases using coagulation model B significantly underpredict CNT length. In these cases sintering has a visible effect for low values of k, where aggregation may still occur before CNT formation, but this effect disappears at higher k values. The effective range for the rate constant is approximately $6 \times 10^{24} - 1 \times 10^{27}$ for cases using coagulation model A. This large range of almost three orders of magnitude suggests the CNT length is insensitive to the actual value, but is instead dictated by time of CNT formation and time of particle deactivation. From equations 10 and 11 the competition between monolayer and CNT growth is clear. Increasing k also increases the rate at which particles are deactivated by carbon coating, hence the insensitivity of CNT length to rate constant. The effect of sintering is again clearly seen as it reduces CNT length at lower rate constants. This can be explained by the lower surface area of sintered catalyst particles reducing the CO process rates.

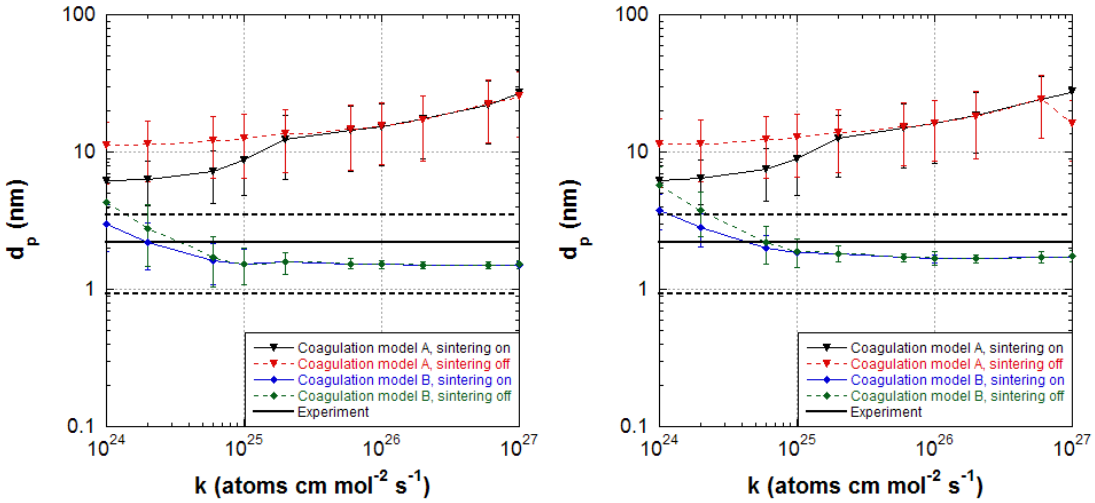

(a) Inception model I

(b) Inception model II

Figure 8: *Average particle diameter after* 5 *s flow time for different CO rate constants. Horizontal lines show experimental average (solid) and standard deviation (dotted). Bars show standard deviations.*

6 CNT Inception Model Comparison

Particle diameter, d_p, CNT diameter, d_{cnt}, and CNT length, L, were chosen to characterise the simulation predictions, as all three variables were available experimentally. The two proposed CNT inception models were compared. Model I allows CNTs to form after a particle becomes saturated, and model II only allows a CNT to form on the collision of two saturated particles (Height hypothesis [9]). Simulations were performed using the initial estimate for k, and using the most appropriate value from the parameter study; $k = 6 \times 10^{24}$.

Figure 11 shows the particle size distribution for the different CNT inception models for the initial estimate rate constant, and the most appropriate value from the parameter study. Clearly the CNT inception model has no effect on the particle size distribution. Decreasing the rate constant to 6×10^{24} brings the simulations slightly closer to the experimental data, but the values are still overpredicted by about four times.

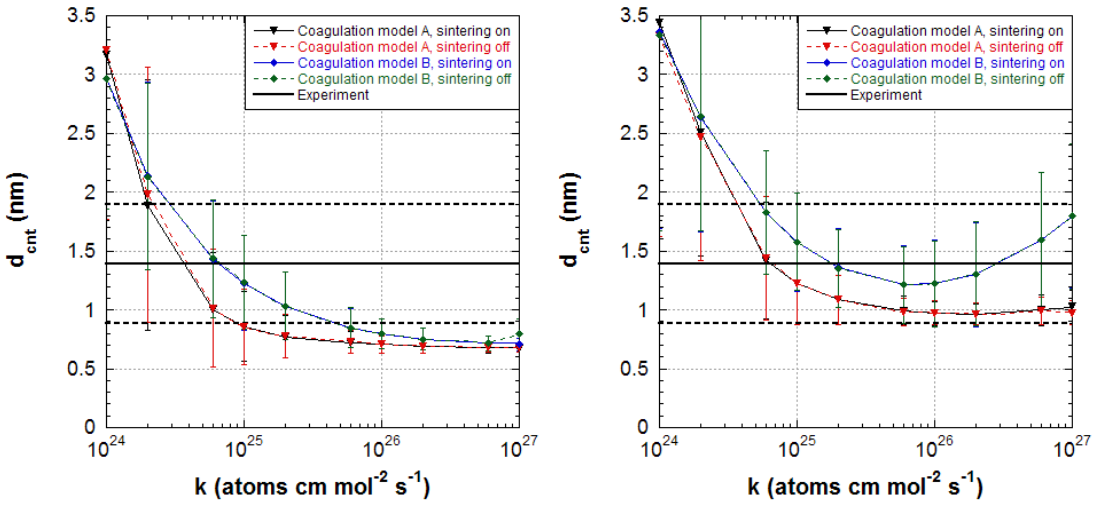

(a) Inception model I (b) Inception model II

Figure 9: *Average CNT diameter after* 5 *s flow time for different CO rate constants. Horizontal lines show experimental average (solid) and standard deviation (dotted).*

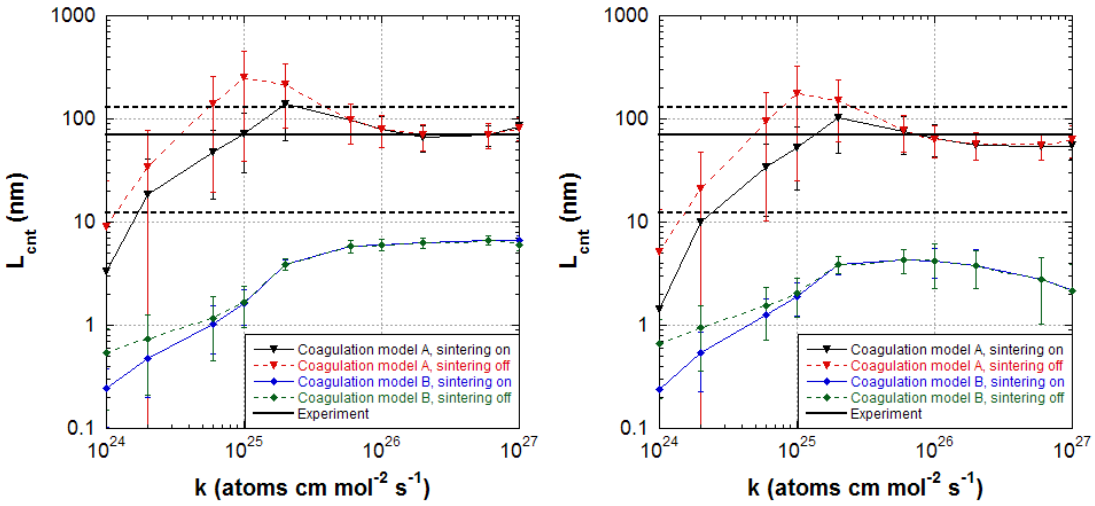

(a) Inception model I (b) Inception model II

Figure 10: *Average CNT length after* 5 *s flow time for different CO rate constants. Horizontal lines show experimental average (solid) and standard deviation (dotted).*

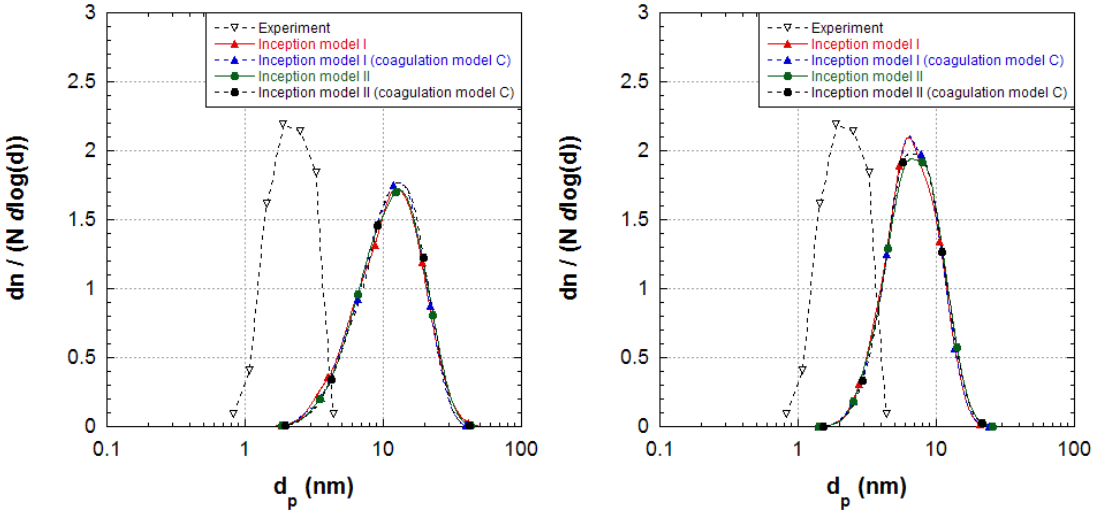

(a) $k = 2 \times 10^{25}$ (b) $k = 6 \times 10^{24}$

Figure 11: *Particle diameter distribution for different CNT inception models.*

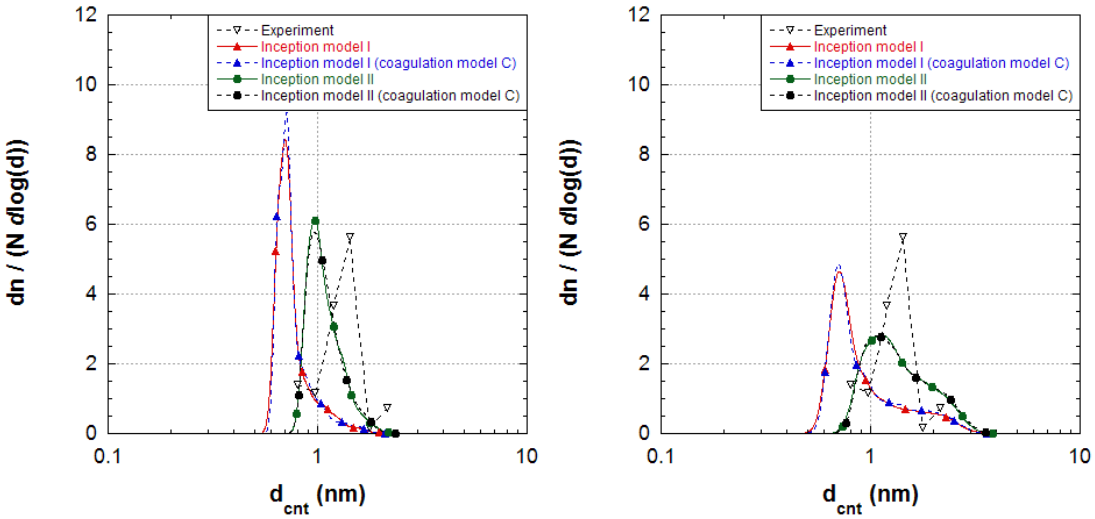

(a) $k = 2 \times 10^{25}$ (b) $k = 6 \times 10^{24}$

Figure 12: *CNT diameter distribution for different CNT inception models.*

Figure 12 shows the CNT diameter distribution for the two inception models. There is a clear difference between the inception models. Model II is a far better fit to the experiments than model I. Changing from coagulation model A to model C has no noticeable effect on CNT diameter.

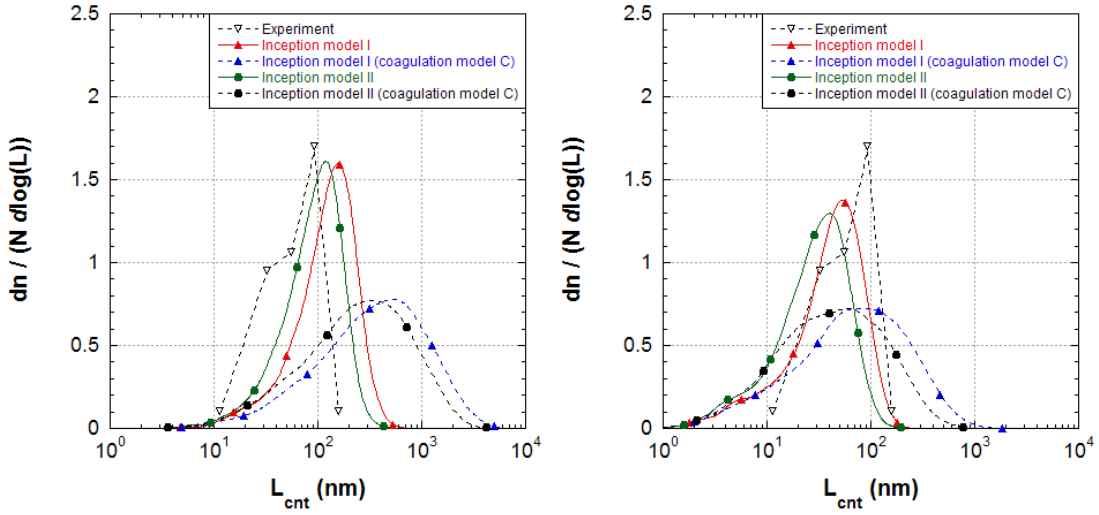

(a) $k = 2 \times 10^{25}$ (b) $k = 6 \times 10^{24}$

Figure 13: *CNT length distribution for different CNT inception models.*

Figure 13 shows the CNT length distributions for the two inception models. The two models agree quite closely, and any difference can probably be attributed to the difference in CNT diameter. Using coagulation model C increases the length of CNTs for both models. This is expected as model C does not discard CNTs on the collision of two particles with CNTs. The CNTs are instead added together, giving longer CNTs. Using the initial estimate for k, the simulations suggest the coagulation model A is more appropriate, however, when $k = 6 \times 10^{24}$ either coagulation model could be used to represent the data, given the simplicity of the model.

7 Conclusions

A simple model of carbon nanotube growth for gas-phase synthesis has been introduced and studied. CO disproportionation and hydrogenation were modelled as the only processes to form CNTs. This model was successfully solved using a stochastic population balance solver coupled to the gas-phase chemistry by operator splitting.

A parameter study of CO reaction rate constant k and fraction of carbon going to form CNTs f_{cnt} was conducted. This study also investigated two CNT inception models, two coagulation models and the effects of sintering. This study showed that the initial estimates of $k = 2 \times 10^{25}\ \mathrm{atoms\,cm\,mol^{-2}\,s^{-1}}$ and $f_{cnt} = 0.5$ could represent the experimental data reasonably well, though a better fit was achieved using a rate constant of

$k = 6 \times 10^{24}\,\mathrm{atoms\,cm\,mol^{-2}\,s^{-1}}$. The simulations captured the CNT length distribution well for all models, however, catalyst particle diameter was overpredicted by about an order of magnitude when coagulation was allowed, but agreed well when coagulation was disallowed. CNT diameter was consistently underpredicted except at very low values of k. When coagulation was disallowed (model B), CNT length was grossly underpredicted.

Two CNT inception models were considered. The first model allows CNTs to form as soon as a particle reaches saturation (model I), depending on the rate of carbon addition. The second model only allows a CNT to form on the collision of two saturated catalyst particles (model II). The simulations showed no discernable difference between the models for the prediction of particle diameter and CNT length, however, inception model II was better at matching CNT diameter. Table 3 summarises the most suitable models to match the experimental data, as predicted by this study.

Table 3: *Summary of most suitable models to match experimental data.*

Variable to Match	Inception Model	Coagulation Model	Sintering Model
Particle diameter, d_p	I or II	B	on
CNT diameter, d_{cnt}	II	A, B or C	on / off
CNT length, L_{cnt}	I or II	A or C	on

This paper provides the ground work for future studies of gas-phase CNT synthesis and has shown that simulations of these highly complex, multivariate systems are possible. Several areas of future research have been highlighted by this work. The rate description for CO disproportionation and hydrogenation is perhaps oversimplified, and could benefit from a more thorough consideration, perhaps to include a temperature dependence, reversibility and diffusive transport limitations. The surface-volume particle model is also too simplistic to capture all aspects of CNT-particle interactions. A full 3D structure model [16] should allow significantly more detailed simulations, in particular it would allow CNT bundles to be modelled. The coagulation kernel used was developed for spherical particles, and hence does not describe CNTs well at all. This must be investigated. Also, a more advanced CNT description is required to look at properties such as chirality and the propensity to form CNT bundles. The consistent underprediction of CNT diameter suggests that the point of CNT inception is incorrect and must be investigated further. The current model is overidealistic in that it does not account for catalyst particle size or shape in determining whether or not a CNT may form. Nonetheless, the fact that the model is in semiquantitative agreement with experiment suggests that it captures most of the important physics in these interesting systems.

References

[1] Hiroki Ago, Naoyasu Uehara, Naoki Yoshihara, Masaharu Tsuji, Motoo Yumura, Nariyuki Tomonaga, and Toshihiko Setoguchi. Gas analysis of the CVD process for high yield growth of carbon nanotubes over metal-supported catalysts. *Carbon*, 44: 2912–2918, 2006.

[2] M Balthasar and M Kraft. A stochastic approach to solve the particle size distribution function of soot particles in laminar premixed flames. *Combust. Flame*, 133:289–298, 2003.

[3] K. Bladh, L.K.L. Falk, and F. Rohmund. On the iron-catalysed growth of single-walled carbon nanotubes and encapsulated metal particles in the gas phase. *Appl. Phys. A: Materials Science & Processing*, 70:317–322, 2000.

[4] Robert L. Carver, Haiqing Peng, Anil K. Sadana, Pasha Nikolaev, Sivaram Arepalli, Carl D. Scott, W. E. Billups, Robert H. Hauge, and Richard E. Smalley. A model for nucleation and growth of single wall carbon nanotubes via the HiPco process: A catalyst concentration study. *J. Nanosci. Nanotech.*, 5:1035–1040, 2005.

[5] Matthew Celnik, Robert Patterson, Markus Kraft, and Wolfgang Wagner. Coupling a stochastic soot population balance to gas-phase chemistry using operator splitting. *Combust. Flame*, 148(3):158–176, 2007.

[6] Feng Ding, Arne Rosén, and Kim Bolton. Molecular dynamics study of the catalyst particle size dependence on carbon nanotube growth. *J. Chem. Phys.*, 121(6):2775–2779, 2004.

[7] J. Gavillet, A. Loiseau, F. Ducastelle, S. Thair, P. Bernier, O. Stephan, J. Thibault, and J.-C. Charlier. Microscopic mechanisms for the catalyst assisted growth of single-wall carbon nanotubes. *Carbon*, 40:1649–1663, 2002.

[8] T. Guo, P. Nikolaev, A. Thess, D.T. Colbert, and R.E. Smalley. Catalytic growth of single-walled nanotubes by laser vaporization. *Chem. Phys. Letters*, 243:49–54, 1995.

[9] Murray Height. *Flame Synthesis of Carbon Nanotubes and Metallic Nanomaterials*. PhD thesis, Massachusetts Institute of Technology, 2003.

[10] A. Maiti, C. J. Brabec, and J. Bernholc. Kinetics of metal-catalyzed growth of single-walled carbon nanotubes. *Phys. Rev. B*, 55(10):R6097–R6100, 1997.

[11] Shigeo Maruyama, Yoichi Murakami, Yasushi Shibuta, Yuhei Miyauchi, and Shohei Chiashi. Generation of single-walled carbon nanotubes from alcohol and generation mechanism by molecular dynamics simulations. *J. Nanosci. Nanotech*, 4(4):360–367, 2004.

[12] Anna Moisala, Albert G Nasibulin, and Esko I Kauppinen. The role of metal nanoparticles on the catalytic production of single-walled carbon nanotubes - a review. *J. Phys. Condensed Matter*, 15:S3011–S3035, 2003.

[13] Anna Moisala, Albert G Nasibulin, Sergei D. Shandakov, Hua Jiang, and Esko I Kauppinen. On-line detection of single-walled carbon nanotube formation during aerosol synthesis methods. *Carbon*, 43:2066–2074, 2005.

[14] Anna Moisala, Albert G Nasibulin, David P. Brown, Hua Jiang, Leonid Khriachtchev, and Esko I Kauppinen. Single-walled carbon nanotube synthesis using ferrocene and iron pentacarbonyl in a laminar flow reactor. *Chem. Eng. Sci.*, 61: 4393–4402, 2006.

[15] Neal Morgan, Clive Wells, Markus Kraft, and Wolfgang Wagner. Modelling nanoparticle dynamics: coagulation, sintering, particle inception and surface growth. *Combust. Theor. Model.*, 9(3):449–461, 2005.

[16] Neal Morgan, Markus Kraft, Michael Balthasar, David Wong, Michael Frenklach, and Pablo Mitchell. Numerical simulations of soot aggregation in premixed laminar flames. *Proc. Comb. Inst.*, 31:693–700, 2007.

[17] H. Mühlenweg, A. Gutsch, A. Schild, and S. E. Pratsinis. Process simulation of gas-to-particle-synthesis via population balances: Investigation of three models. *Chem. Eng. Sci.*, 57:2305–2322, 2002.

[18] Albert G Nasibulin, Anna M Moisala, David P Brown, and Esko I Kauppinen. Carbon nanotubes and onions from carbon monoxide using $Ni(acac)_2$ and $Cu(acac)_2$ as catalyst precursors. *Carbon*, 41:2711–2724, 2003.

[19] Albert G. Nasibulin, Anna Moisala, David P. Brown, Hua Jiang, and Esko I. Kauppinen. A novel aerosol method for single walled carbon nanotube synthesis. *Chem. Phys. Letters*, 402:227–232, 2005.

[20] Albert G Nasibulin, Peter V Pikhitsa, Hua Jiang, and Esko I Kauppinen. Correlation between catalyst particle and single-walled carbon nanotube diameters. *Carbon*, 43: 2251–2257, 2005.

[21] Albert G. Nasibulin, David P. Brown, Paula Queipo, David Gonzalez, Hua Jiang, and Esko I. Kauppinen. An essential role of CO_2 and H_2O during single-walled CNT synthesis from carbon monoxide. *Chem. Phys. Letters*, 417:179–184, 2006.

[22] Albert G Nasibulin, Paula Queipo, Sergei D Shandakov, David P Brown, Hua Jiang, Peter V Pikhitsa, Oleg V Tolochko, and Esko I Kauppinen. Studies on mechanism of single-walled carbon nanotube formation. *J. Nanosci. Nanotech.*, 6:1233–1246, 2006.

[23] Lei Ni, Keiji Kuroda, Ling-Ping Zhou, Tokushi Kizuka, Keishin Ohta, Kiyoto Matsuishi, and Junji Nakamura. Kinetic study of carbon nanotube synthesis over Mo/Co/MgO catalysts. *Carbon*, 44:2265–2272, 2006.

[24] Pavel Nikolaev, Michael J. Bronikowski, R. Kelley Bradley, Frank Rohmund, Daniel T. Colbert, K.A. Smith, and Richard E. Smalley. Gas-phase catalytic growth of single-walled carbon nanotubes from carbon monoxide. *Chem. Phys. Letters*, 313:91–97, 1999.

[25] Robert Patterson, Jasdeep Singh, Michael Balthasar, Markus Kraft, and James Norris. The Linear Process Deferment Algorithm: A new technique for solving population balance equations. *SIAM Journal on Scientific Computing*, (28):303–320, 2006.

[26] Robert Patterson, Jasdeep Singh, Michael Balthasar, Markus Kraft, and Wolfgang Wagner. Extending stochastic soot simulation to higher pressures. *Combust. Flame*, 145(3):638–642, 2006.

[27] Robert Patterson, Jasdeep Singh, Neal Morgan, and Markus Kraft. A simple model for the aggregate structure of soot particles. Technical Report 38, c4e Preprint-Series, Cambridge, 2006.

[28] Carl D Scott and Richard E Smalley. Effects of carbonyl bond, metal cluster dissociation and evaporation rates of predictions of nanotube production in high-pressure carbon monoxide. *J. Nanosci. Nanotech.*, 3(1/2):75–79, 2003.

[29] Carl D Scott, Alexander Povitsky, Christopher Dateo, Tahir Gökçen, Peter A Willis, and Richard E Smalley. Iron catalyst chemistry in modeling a high-pressure carbon monoxide nanotube reactor. *J. Nanosci. Nanotech.*, 3(1/2):63–73, 2003.

[30] John Z Wen, M J Thomson, S H Park, S N Rogak, and M F Lightstone. Study of soot growth in a plug flow reactor using a moving sectional model. *Proc. Comb. Inst.*, 30:1477–1484, 2005.

[31] John Z Wen, F Goldsmith, R Ashcraft, and W H Green. Detailed kinetic modeling of the iron nanoparticle synthesis from the decomposition of $Fe(CO)_5$. *J. Phys. Chem. C*, in press, 2007.

[32] Min-Feng Yu, Mark J Dyer, Jian Chen, Dong Qian, Wing Kam Liu, and Rodney S Ruoff. Locked twist in multiwalled carbon-nanotube ribbons. *Phys. Rev. B*, 64(24): 241403, 2001.